THERMAL STABILITY OF $Au/NbO_x/Nb$ AND $Au/Nb_2O_5/W$ MODEL CATALYSTS STUDIED BY ANGLE-RESOLVED X-RAY PHOTOELECTRON SPECTROSCOPY

Yaroslava LYKHACH[1], Jan PLŠEK[2], Ilona SPIROVOVÁ[3] and Zdeněk BASTL[4,*]

J. Heyrovský Institute of Physical Chemistry, Academy of Sciences of the Czech Republic, Dolejškova 3, 182 23 Prague 8, Czech Republic; e-mail: [1] yaroslava.lykhach@jh-inst.cas.cz, [2] jan.plsek@jh-inst.cas.cz, [3] ilona.spirov@jh-inst.cas.cz, [4] zdenek.bastl@jh-inst.cas.cz

Received June 11, 2003
Accepted August 1, 2003

The thermal stability of gold deposited on Nb_2O_5/W, Nb_2O_5/Nb and NbO/Nb substrates was investigated by angle-resolved X-ray photoelectron spectroscopy. Gold in amounts 0.1–1.2 monolayer was vapour-deposited on an oxide substrate under ultrahigh vacuum. A shift of the Au (4f) core level towards higher binding energies and an increase in the line width with decreasing surface coverage by Au were observed for all supports and explained by final state effects in the photoemission process. The lower magnitude of the shift observed in the case of Au/NbO/Nb was attributed to better screening of the core hole by electrons of the metallic NbO phase. The results present evidence that on heating of the $Au/Nb_2O_5/W$ system up to 550 °C only agglomeration occurred without significant diffusion of Au into the oxide substrate. Annealing of the $Au/Nb_2O_5/Nb$ model catalyst above 350 °C resulted in reduction of Nb_2O_5 to suboxides and inward diffusion of Au. Diffusion into the substrate above 350 °C has also been observed for the Au/NbO/Nb sample. The distribution of Au within the surface layers of substrate has been estimated by analysis of Au (4f) and Nb (3d) angle-resolved spectra. The inward diffusion of Au on annealing observed for the Nb_2O_5/Nb and NbO/Nb substrates is facilitated by a high density of defects in NbO. Besides information on the particular $Au/Nb_2O_5/W$, $Au/Nb_2O_5/Nb$ and Au/NbO/Nb systems, our results demonstrated potentials of angle-resolved photoelectron spectroscopy for determination of the distribution of a metal in annealed model catalysts and for study of extended interfaces.

Keywords: Model metal catalysts; Angle resolved photoemission; Depth profiles; Supported gold; Au/NbO_x interface; Niobium; XPS spectroscopy; Heterogeneous catalysis.

Metals deposited on oxide surfaces are used in many important technological applications including heterogeneous catalysis, fuel cells and microelectronics. In the recent years the catalytic properties of oxide-supported gold have attracted considerable attention. Gold was usually considered as catalytically almost inactive metal. Its low reactivity was attributed to the completely filled 5d atomic orbitals and to its high first ionization potential. However, it follows from calculations[1] that the electronic configuration in

elemental Au is $5d^{9.6}6s^{0.9}6p^{0.5}$. This means that Au should be considered as a metal with unfilled d band, similar to Pd. It was found that in contrast to bulk Au, nanosized gold particles dispersed on various metal oxides can become active in many reactions[2–8]. In particular gold supported on reducible transition metal oxides was found to exhibit a very high catalytic activity[9–11]. The catalytic properties of the dispersed gold depend on the size of gold particles, the preparation method and particularly on the chemical composition of the supporting material which can, among other things, significantly influence the morphology of the particles. It has been suggested[12] that the most important catalytically active sites are located at the perimeters of gold/metal oxide interfaces.

For heterogeneous catalysts based on oxide-supported dispersed metals the thermal stability is a prerequisite. The coagulation and sintering of gold particles is expected to occur when temperature of the catalyst is increased. Furthermore, some of the metal particles may become partially buried or entrapped in the supporting oxide. The above processes lead to a significant decrease in the catalytic activity due to the decrease in the number of available active sites.

Thin oxide films grown under well defined conditions on metallic surfaces are frequently used in basic research as supports for dispersed metals[12,13]. The advantage of such model heterogeneous catalysts is that the problems arising from insulating properties of many oxides can be suppressed or even eliminated allowing thus to use for their study the surface selective experimental techniques like electron and ion spectroscopy methods or scanning tunneling microscopy. However, the detailed investigation of the influence of the oxide layer thickness and of preparation conditions on behavior of such model catalysts have revealed the possibility of incorporation of a fraction of the metal deposited into the oxide substrate even at room temperature[13–16]. Recently[17], using angle-resolved X-ray photoelectron spectroscopy (ARXPS), we observed the inward diffusion of palladium caused by heating of the $Pd/Nb_2O_5/Nb$ model catalyst at temperatures above 320 °C. This finding allowed to explain a significant decrease of CO adsorption observed on annealed samples.

The present paper is aimed at gaining a better understanding of the effects taking place during annealing of the $Au/NbO_x/Nb$ and $Au/Nb_2O_5/W$ model catalysts. Niobium oxide support was chosen because it is a typical example of SMSI (strong metal–support interaction) support, which can be relatively easily reduced and reoxidized.

EXPERIMENTAL

The angle-resolved XPS measurements were carried out using ESCA 310 (Gammadata Scienta) electron spectrometer equipped with a high-power rotating anode and with a wide-angle X-ray quartz monochromator. Some experiments with Nb_2O_5/W substrates were performed in an ESCA 3 MkII (VG Scientific) electron spectrometer. The pressure of residual gases in the analyzer chamber during spectra acquisition was below 10^{-8} Pa. Nb_2O_5 layers, 2–12 nm thick, were either deposited by sublimation from tungsten filament onto W substrate cleaned by argon ion sputtering or was grown in the preparation chamber of the spectrometer as a thin layer by oxidizing pure Nb (99.9%, Leybold–Heraeus) polycrystalline foil 0.2 mm thick. Prior to oxidation the foil surface was cleaned by argon ion sputtering. NbO/Nb substrate was prepared by heating the Nb_2O_5/Nb sample to 550 °C for 1 h in the preparation chamber of the spectrometer at pressure 10^{-7} Pa. Controlled amounts of gold (99.99%; Aldrich Chem. Co.) were deposited onto niobium oxide surface in the preparation chamber of the spectrometer at a pressure lower than 2×10^{-8} Pa from a resistively heated and thoroughly outgassed tungsten filament wrapped with 0.1 mm diameter Au wire. During deposition the substrate was kept at room temperature. High resolution spectra of Nb (3d), Au (4f) and O (1s) core electrons and valence band electrons were measured at several take-off angles. The estimated error in the determination of the core-level binding energies did not exceed ±0.1 eV. The samples were gradually heated in ultrahigh vacuum up to 550 °C and kept at each selected temperature for 1 h. For spectra acquisition the samples were cooled down to room temperature.

The thickness of the oxide layer was calculated from intensities of Nb (3d) photoemission lines using a simple layer model[18]. In these calculation we used theoretical values of photoionisation cross-sections published by Scofield[19] and electron inelastic mean free paths values calculated from the TPP-2M equation[20]. For atomic (molecular) concentrations the values calculated from the density and atomic (molecular) mass were adopted (N(Au) = 5.9×10^{22}, N(Nb) = 5.55×10^{22}, $N(Nb_2O_5) = 1.04 \times 10^{22}$ and N(NbO) = 4.04×10^{22} cm^{-3}). The Au coverage was expressed in monolayer equivalent units (ML) even if Au does not necessarily grow on the used substrates in a layer-by-layer mode. The concentration depth profiles of Au were analyzed using the procedures described in the literature[21] and the Cumpson-type[22] profile.

The contribution of the Au deposit to the valence band photoemission was determined by subtracting a suitably attenuated spectrum of a clean substrate surface. The attenuation was determined from intensities of the Nb (3d) spectra assuming that the spectra of valence electrons and Nb (3d) electrons are affected by the Au deposit to the same extent. Implicit in this procedure is also the assumption that the shape of the substrate spectrum is not significantly modified by the deposited Au.

RESULTS AND DISCUSSION

In order to study the growth of Au on niobia, the Nb_2O_5/Nb and Nb_2O_5/W substrates were first prepared and examined *in situ* by means of ARXPS. High-resolution spectra of the Nb (3d) electrons taken from Nb_2O_5/Nb and Nb_2O_5/W samples are shown in Fig. 1. The main difference between the two metal substrates consists in different thermal stability of Nb_2O_5 layer. As reported in our previous paper[17], heating of the Nb_2O_5/Nb system to

550 °C leads to transformation of Nb_2O_5 to NbO. However, Nb_2O_5/W is quite stable and only narrowing of the Nb (3d) spectrum components and the downward shift by 0.15 eV occurs on heating to 550 °C. The observed spectral changes are most likely due to the transformation of partially disordered oxide into a more ordered modification with more homogeneous environment of Nb ions. The deconvolution of the Nb (3d) spectra revealed the presence of several components. In agreement with our previous results[17], besides the main peaks centered at 207.6 and 202.2 eV belonging to Nb_2O_5 and to metallic Nb, respectively, we observed the components located at 206.2, 203.0 and 204.0 eV which could be assigned, respectively, to NbO_2, NbO and NbO_x. In contrast to the Nb_2O_5/Nb sample, the spectrum of Nb (3d) electrons measured for Nb_2O_5/W substrate shows only a minor contribution of Nb suboxides. Intensity variations of the suboxide components in the angle-resolved spectra of the Nb (3d) electrons indicate that suboxides are located at the W-metal/oxide interface where they are produced by reaction of Nb_2O_5 with surface atoms of W support.

The changes in the Au (4f) and Nb (3d) core level emission were monitored during the stepwise deposition of Au. The dependence of the Au ($4f_{7/2}$) core-level binding energy (BE) and the full width of the peak at half maximum (FWHM) on Au coverage are presented in Figs 2 and 3, respectively. The general trends of BE and FWHM variations in dependence on

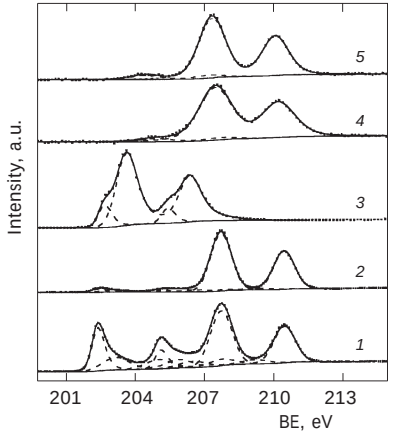

FIG. 1

Spectra of the Nb (3d) photoelectrons taken from: *1* Nb_2O_5/Nb (oxide thickness d_{ox} = 7 nm, 25 °C); *2* Nb_2O_5/Nb (d_{ox} = 12 nm, 25 °C); *3* Nb_2O_5/Nb (after heating sample *2* to 550 °C for 1 h, thickness of resulting NbO d_{ox} = 5.7 nm); *4* Nb_2O_5/W (d_{ox} = 3 nm, 25 °C); *5* sample *4* after heating to 550 °C for 1 h

the surface coverage are qualitatively similar to those reported for the dispersed gold and some other metals on oxide surfaces[23–30], *i.e.* an increase of the BE and FWHM with decreasing surface coverage by Au. The shifts of BE as well as FWHM obtained for Nb_2O_5/Nb and Nb_2O_5/W substrates are the same within the experimental error. The smaller BE shifts and higher

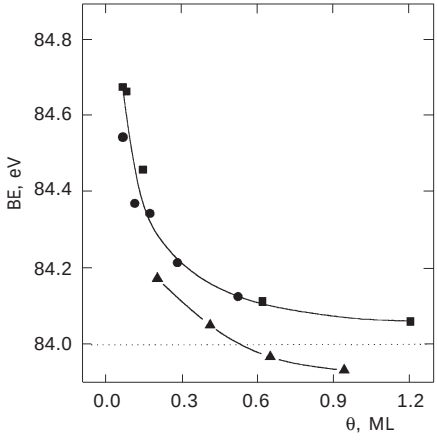

FIG. 2
The dependence of the Au ($4f_{7/2}$) core-level BE on surface gold coverage θ for: Au/Nb_2O_5/Nb, d_{ox} = 7 nm (■); Au/Nb_2O_5/W, d_{ox} = 3 nm (●); Au/NbO/Nb, d_{ox} = 5.7 nm (▲)

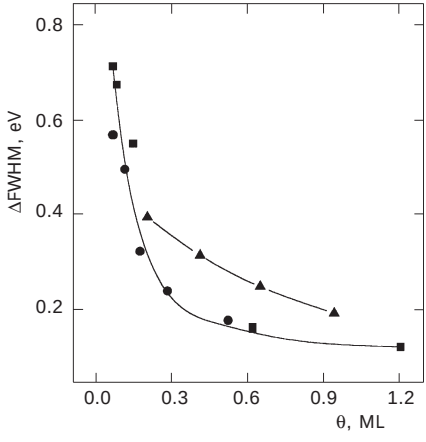

FIG. 3
The dependence of the difference of the Au ($4f_{7/2}$) line width ΔFWHM between the deposited and bulk Au on surface gold coverage θ for: Au/Nb_2O_5/Nb, d_{ox} = 7 nm (■); Au/Nb_2O_5/W, d_{ox} = 3 nm (●); Au/NbO/Nb, d_{ox} = 5.7 nm (▲)

FWHM were observed during Au deposition on the NbO/Nb substrate (Figs 2 and 3) For gold surface coverage $\theta > 0.5$ ML, even negative BE shifts with respect to the bulk value were measured amounting to –0.05 eV for $\theta = 1$ ML.

The measured shifts of the Au (4f) core-level BE contain two contributions, the initial state contribution related to the orbital energy of the photoemitted electron and the contribution due to final state effects corresponding to the energy difference between the excited electron system after photoemission and the relaxed system. In addition, for insulating supports, charging of the Au particles is caused by photoemission leading to the increase of the core-level BE due to Coulombic attraction between the charged particle and the outgoing electron. The measured BE shifts then depend on the ability of the support to neutralize the particle charge within the core hole lifetime, which in turn depends on the electronic structure of the supporting material, metal particle size and particle morphology.

There is a redistribution of electrons between 6s and 5d states of Au for surface atoms, which leads to a shift of the core-level BEs towards lower values compared with the bulk value[26]. Since the fraction of the surface atoms with lower coordination increases with decreasing size of Au particles, we would expect the core-level BE to decrease with decreasing amount of Au deposited. Consequently, the observed increase of Au (4f) core-level BE in the region of low surface coverage is likely due to the final state effects which exceed the decrease caused by reduced coordination of Au atoms. The smaller and for $\theta > 0.5$ ML even negative BE shift observed for Au/NbO/Nb then can tentatively be attributed to better screening of the core hole due to metallic properties[30] of NbO.

The origin of positive core level shifts in Au dispersed on TiO_2 and MgO oxides has been recently calculated using the density functional method[31]. The authors came to the conclusion that at a low surface coverage, the presence of surface oxygen vacancies rather than core hole relaxation is responsible for positive BE shifts observed in experiments. The role of oxygen vacancies has also been discussed by other authors[32,33] but unequivocal explanation has not yet been obtained.

Thermal Stability of $Au/NbO_x/Nb$ and $Au/Nb_2O_5/W$ Systems

The study of the thermal stability of Au deposited on Nb_2O_5/Nb, Nb_2O_5/W and NbO/Nb substrates has been performed using ARXPS. For these experiments we used the samples Au/Nb_2O_5/Nb with approximately 1 ML cover-

age of Au prepared by the stepwise deposition of Au as described above. The effect of annealing was examined at four different temperatures.

Figure 4 shows variations of BE and FWHM of the Au ($4f_{7/2}$) photoelectron line with temperature for Au/Nb_2O_5/Nb. Heating to 250 °C resulted in broadening of the Au ($4f_{7/2}$) line without changes of the Au ($4f_{7/2}$) core-level BE. The broadening of the Au ($4f_{7/2}$) line continues at 350 °C and the BE of ($4f_{7/2}$) electrons at this temperature increases to 84.5 eV. The temperature of approximately 350 °C represents the break-point in the behavior of Au (4f) spectral parameters. Further increase of temperature is accompanied by increase of the Au ($4f_{7/2}$) BE and decrease of FWHM.

The influence of annealing on Au (4f) to Nb^0 (3d) peak intensity ratio is shown in Fig. 5 for the two detection angles corresponding to perpendicular photoemission and photoemission at 60° (defined from the normal to the sample surface). The data in Fig. 5 show that the Au (4f)/Nb^0 (3d) intensity ratio decreases on annealing of the sample and ratios obtained at the two different detection angles become rather close for annealing temperatures above 350 °C. Note that independence of composition on the take-off angle is characteristic of the samples homogeneous within the depth analyzed by the XPS method.

Based on the measured changes of the spectral parameters we can qualitatively divide the development of the Au deposit morphology with temperature into two regions. In the first region, up to 350 °C, the changes in Au

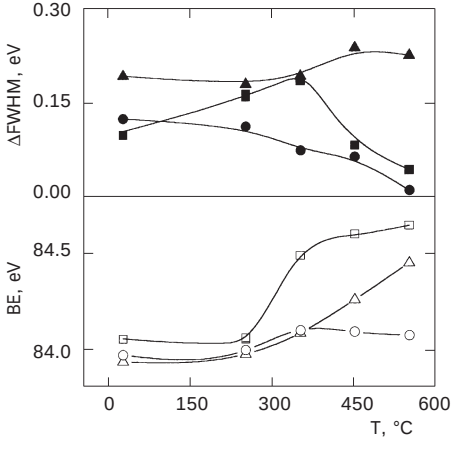

FIG. 4
The dependence of the Au ($4f_{7/2}$) core-level BE (open symbols) and the difference in the line width ΔFWHM (solid symbols) on the substrate temperature *T* for: Au/Nb_2O_5/Nb (■); Au/Nb_2O_5/W (●); Au/NbO/Nb (▲)

($4f_{7/2}$) BE and FWHM can be tentatively explained by redispersion of the Au deposit resulting in broadening of the particle size distribution. In the second region, at temperatures above ≈350 °C Au prefers to be driven into the oxide substrate instead staying on the surface. The inward diffusion of Au can eventually result in formation of the Au-Nb alloy at the Nb-oxide/Nb-metal interface. This behavior is similar to that found for the $Pd/Nb_2O_5/Nb$ system[17]. The described redispersion of Au and its subsequent incorporation into the support is accompanied by reduction of Nb_2O_5 oxide layer due to oxygen dissolution in the underlying Nb metal taking place at temperatures above 280 °C as shown in Fig. 6. This process is demonstrated by the presence of several Nb-oxide components in the spectra of the Nb (3d) electrons. The Nb_2O_5 oxide is transformed to NbO above 350 °C. At the same temperature the inward Au diffusion begins (see Fig. 5). It is known[30] that NbO contains a high number of vacancies, the highest number found among transition metal monoxides. We suppose that these vacancies considerably enhance inward diffusion of Au.

In order to elucidate the influence of the supporting oxide composition on the Au diffusion, we also studied the thermal behavior of Au deposited on Nb_2O_5/W and NbO/Nb substrates with oxide thickness 3 and 5.7 nm, respectively. The thermal stability studies were performed with depositions of 1.5 ML of Au on Nb_2O_5/W and 0.94 ML of Au on NbO/Nb. As already mentioned, the changes of the Au (4f) BE in dependence on surface coverage are the same for $Au/Nb_2O_5/Nb$ and $Au/Nb_2O_5/W$ systems (see Figs 2

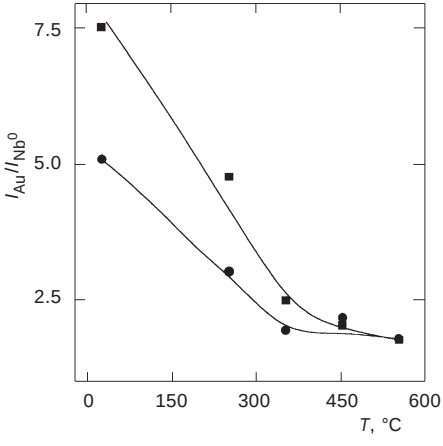

FIG. 5

The dependence of the Au (4f)/Nb (3d) intensity ratio for $Au/Nb_2O_5/Nb$, d_{ox} = 5.7 nm, on temperature measured at two different take-off angles: 60° (■), 0° (●)

and 3). However, the changes of BE and FWHM occurring during annealing of the samples (Fig. 4) are different. Heating up to 550 °C results in a rather small increase (0.1 eV) of the BE of Au ($4f_{7/2}$) electrons for the Au/Nb_2O_5/W sample and narrowing of the Au ($4f_{7/2}$) line. This behavior can be explained by agglomeration of Au in the course of which larger Au particles grow at the expense of the small ones (Ostwald ripening) and is in accord with measured decrease of Au (4f) spectra intensity. Consequently, the total number of surface gold atoms with reduced coordination decreases leading thus to the observed small increase of Au ($4f_{7/2}$) BE.

A different result was found for the Au/NbO/Nb sample for which the total BE shift of Au (4f) spectra caused by a temperature increase from 25 to 550 °C is 0.52 eV and the Au ($4f_{7/2}$) line slightly broadens. The value of the BE shift is close to that measured for the Au/Nb_2O_5/Nb system for which an increase of 0.6 eV was obtained (Fig. 4).

The intensity of the Au (4f) spectra decreases with increasing temperature for Au/NbO/Nb samples. This decrease can be caused by Au agglomeration on the support surface as well as by the inward diffusion of Au. To distinguish between the two possibilities, we explored the angle-resolved XP spectra. In Fig. 7, the dependence of the Au (4f) line intensities divided by the sum of Au (4f) and Nb (3d) spectra intensities (all normalized to the pertinent photoionization cross-sections) on the take-off angle is demonstrated for the used annealing temperatures. For analysis of the angle-resolved data, the equation describing intensity of the deposit photo-

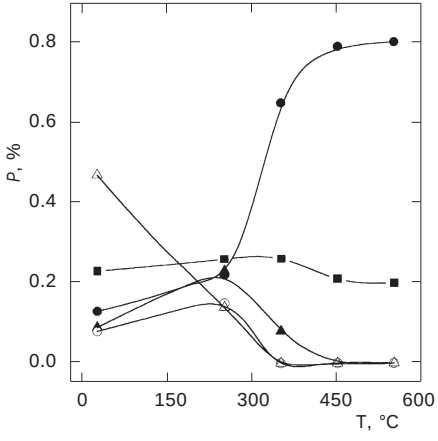

FIG. 6

The dependence of population of the individual oxidation states of Nb on temperature. Nb^0 (■), Nb^{2+} (●), Nb^{x+} (▲), Nb^{4+} (○) and Nb^{5+} (△) for Au/Nb_2O_5/Nb

emission line for a substrate partially covered by the deposited material and published by Paynter[21] can be used:

$$\frac{I(\alpha)}{\phi TA\sigma \cos\alpha} = f\left\{c_L \lambda_L \left[1 - e^{\frac{t}{\lambda_L \cos\alpha}}\right] + c_S \lambda_S e^{\frac{t}{\lambda_L \cos\alpha}}\right\} + (1-f) c_S \lambda_S \,, \qquad (1)$$

where ϕ is the X-ray flux, α is the detection angle defined from the normal to the sample surface, T is the transmission efficiency, A is the analysis area, σ is the cross-section for photoelectron emission, f is the fraction of the substrate surface covered by the deposited metal, λ_L and λ_S are the inelastic mean free paths of Au (4f) photoelectrons in the deposited Au and in NbO substrate, respectively, c_L and c_S are the concentrations of Au present on the oxide surface and incorporated in the oxide, respectively and t is deposit thickness.

Equation (*1*) can be rewritten to:

$$\frac{I(\alpha)}{\phi TA\sigma} = f c_L \lambda_L \cos\alpha + (1-f) c_S \lambda_S \cos\alpha - f(c_L \lambda_L - c_S \lambda_S) \cos\alpha \, e^{\frac{t}{\lambda_L \cos\alpha}} \,. \qquad (2)$$

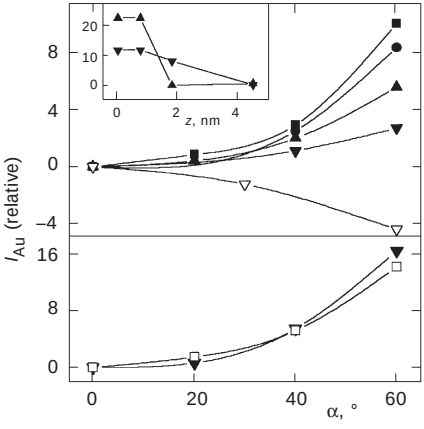

FIG. 7

The dependence of the normalized intensity of the Au (4f) spectra $I^n_{Au} = [(I_{Au} / \sigma_{Au}) / (I_{Au} / \sigma_{Au} + I_{Nb} / \sigma_{Nb})] \times 100$ on detection angle and substrate temperature. The upper part shows the results for Au/NbO/Nb (■ 250 °C, ● 350 °C, ▲ 450 °C, ▼ 550 °C) and Au/Nb_2O_5/Nb (▽ 550 °C). The concentration depth profile of Au calculated using the Cumpson-type profile for Au/NbO/Nb is depicted in the inserted graph for the two substrate temperatures (▲ 450 °C, ▼ 550 °C). In the lower part the results for Au/Nb_2O_5/W are displayed (▼ 550 °C, □ 25 °C)

It follows from Eq. (*2*) that changes of the Au (4f) photoemission intensity during annealing can be caused by variations of f, c_L and c_S. To get rid of the first two terms in Eq. (*2*) the data for each temperature were vertically shifted in such a way that the normalized intensity of the Au (4f) photoemission in normal direction was set to zero (Fig. 7).

It can be seen from Fig. 7 that the results obtained for different substrates are different. In contrast to almost identical exponential dependences obtained for $Au/Nb_2O_5/W$ at temperatures 25 and 550 °C, the slopes of the curves decrease with increasing temperature of annealing for Au/NbO/Nb.

Considering the influence of the pre-exponential factor consisting of f and the difference of atomic concentrations of Au multiplied by corresponding electron inelastic mean free paths in the deposit and the substrate ($c_L\lambda_L - c_S\lambda_S$), it can be shown that the influence of the latter is more pronounced. The trends in exponential dependences for Au/NbO/Nb and $Au/Nb_2O_5/W$ systems can thus be explained by a decrease in the difference ($c_L\lambda_L - c_S\lambda_S$). This decrease is in the case of Au/NbO/Nb due to the inward diffusion of Au leading to the increase in c_S at the expense of c_L, the process which does not take place in the case of the $Au/Nb_2O_5/W$ sample. It should be mentioned that if $c_L\lambda_L < c_S\lambda_S$, the sign of pre-exponential changes to negative, which is likely the case of the $Au/Nb_2O_5/Nb$ sample. Using the Cumpson-type profile[22], we have calculated the depth distribution of Au for Au/NbO/Nb sample. The resulting profiles obtained for temperatures 450 and 550 °C included in Fig. 7 clearly demonstrate inward diffusion of Au on annealing.

The separation of the components of the Nb (3d) spectra belonging to Nb^{2+} and Nb^0 oxidation states increases with increasing annealing temperature starting at 350 °C (see Table I). Change in the separation between metal and oxide photoemission peaks has already been reported in the literature[14] for the $Au/Al_2O_3/Al$ system and explained by the authors in terms of a change in electron extraatomic relaxation.

The spectra of the valence electrons measured for the Au/NbO/Nb system after annealing and corrected for the contribution of the NbO/Nb substrate are displayed in Fig. 8 in which the spectra obtained for the two different Au depositions and for the polycrystalline Au foil with a clean surface are also shown. The splittings of the Au (5d) components, Δ5d, and the Au (5d) bandwidths, W, are given in Table I. With increasing surface coverage by Au, the 5d band splitting as well as the bandwidth increases, due to the increase in the average coordination number of Au atoms. The other interesting observation in Fig. 8. is that heating of the sample first leads to an increase of the Δ5d and W values whereas a decrease is observed at tempera-

tures above 350 °C. At the same time, the high-energy component of the Au (5d) band shifts by 0.5 eV towards higher binding energies. This shift is the same as that of the Au ($4f_{7/2}$) core level. The observed behavior is thus in good agreement with the above given picture of gradual incorporation of the deposited Au atoms in the supporting oxide resulting ultimately in the formation of Au-Nb alloy-like phase. This interpretation is corroborated by the results of electric-resistance study[34] of Au/Nb films in dependence on

TABLE I
Splittings of the Au (5d) band Δ5d, valence bandwidths *W* and separation of the Nb^{2+} and Nb^0 components in the Nb (3d) spectra δ for Au/NbO/Nb system

θ, ML	*T*, °C	Δ5*d*, eV	*W*, eV	δ, eV
0.4	25	2.44	4.50	0.96
0.94	25	2.70	4.82	0.96
0.94	250	2.86	4.97	0.97
0.94	350	2.70	5.01	1.00
0.94	450	2.49	4.65	1.04
0.94	550	2.18	4.14	1.08
Bulk Au	25	3.04	5.23	–

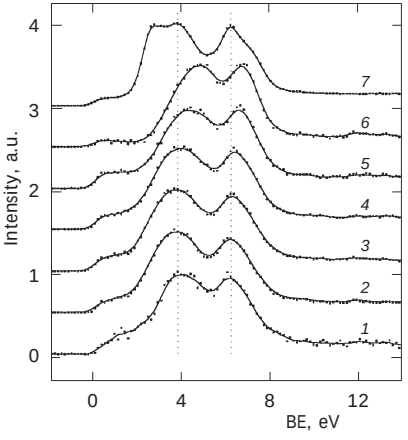

FIG. 8
Valence band X-ray photoemission spectra of Au/NbO/Nb. *1* 0.4 ML; *2* 0.94 ML; *3* 0.94 ML, 250 °C; *4* 0.94 ML, 350 °C; *5* 0.94 ML, 450 °C; *6* 0.94 ML, 550 °C; *7* polycrystalline bulk gold

the annealing temperature. Interdiffusion between the Au and Nb metal films was detected at temperatures above 325 °C and formation of the intermetallic Au_2Nb_3 compound and some other unknown phases was observed above 400 °C.

CONCLUSIONS

The thermal stability of Au/Nb_2O_5/Nb, Au/Nb_2O_5/W and Au/NbO/Nb model supported catalysts containing approximately 1 ML of Au was studied in the temperature range 25–550 °C by the angle-resolved XPS method. The inward diffusion at temperatures above 350 °C was observed for Au/Nb_2O_5/Nb and Au/NbO/Nb but not for Au/Nb_2O_5/W. The depth distribution of Au in the annealed Au/NbO/Nb model catalyst has been determined. It is concluded that the reduction of Nb_2O_5 to NbO oxide gives rise to the inward diffusion of Au in the Au/Nb_2O_5/Nb sample due to high density of defects in NbO.

We gratefully acknowledge the support of this work by the Grant Agency of the Czech Republic (grants No. 104/02/0664 and No. 202/98/K002).

REFERENCES

1. Mattheis L. F., Dietz R. E.: *Phys. Rev. B* **1980**, *22*, 1663.
2. Haruta M.: *Catal. Today* **1997**, *36*, 153.
3. Valden M., Lai X., Goodman D. W.: *Science* **1998**, *281*, 1647.
4. Bond G. C., Thompson D. T.: *Catal. Rev.–Sci. Eng.* **1999**, *41*, 319.
5. Haruta M., Date M.: *Appl. Catal., A* **2001**, *222*, 427.
6. Grisel H., Nienwenhuys B. E.: *Catal. Today* **2001**, *64*, 69.
7. Bond G. C.: *Catal. Today* **2002**, *72*, 5.
8. Scire S., Minico S., Crisafulli C., Satriano C., Pistone A.: *Appl. Catal., B* **2003**, *40*, 43.
9. Haruta M., Yamada N., Kobayashi T., Iijima S.: *J. Catal.* **1989**, *115*, 301.
10. Dekker M. A. P., Lippits M. J., Niewenhuys B. E.: *Catal. Today* **1999**, *54*, 381.
11. Grunwaldt J. D., Baiker A.: *J. Phys. Chem.* **1999**, *103*, 1002.
12. Campbell C. T.: *Surf. Sci. Rep.* **1997**, *27*, 3.
13. Bäumler M., Freund H.-J.: *Prog. Surf. Sci.* **1999**, *61*, 127.
14. Ocal C., Ferrer S., Garcia N.: *Surf. Sci.* **1985**, *163*, 335.
15. Mayer J. T., Lin R. F., Garfunkel E.: *Surf. Sci.* **1992**, *265*, 102.
16. Šarapatka T. J.: *J. Electron Spectrosc. Relat. Phenom.* **1993**, *562*, 335.
17. Thiam M. M., Bastl Z.: *Surf. Sci.* **2002**, *507*, 678.
18. Bastl Z., Senkevich A. I., Spirovová I., Vrtílková V.: *Surf. Interface Anal.* **2002**, *34*, 477.
19. Scofield J. H.: *J. Electron Spectrosc. Relat. Phenom.* **1976**, *8*, 129.
20. Tanuma S., Powell C. J., Penn D. R.: *Surf. Interface Anal.* **1994**, *21*, 165.
21. Paynter R. W.: *Surf. Interface Anal.* **1999**, *27*, 103.

22. Cumpson P.: *J. Electron Spectrosc. Relat. Phenom.* **1995**, *73*, 25.
23. Lee S. T., Apai G., Mason M. G.: *Phys. Rev. B: Condens. Matter* **1981**, *23*, 505.
24. Mason M. G.: *Phys. Rev. B: Condens. Matter* **1983**, *27*, 748.
25. Oberli L., Monot R., Mathieu H. J., Landolt D., Buffet J.: *Surf. Sci.* **1981**, *106*, 301.
26. Citrin P. H., Wertheim G. K.: *Phys. Rev. B: Condens. Matter* **1983**, *27*, 3176.
27. Wertheim G. K., DiCenzo S. B: *Phys. Rev. B: Condens. Matter* **1988**, *37*, 844.
28. Bastl Z.: *Vacuum* **1986**, *36*, 447.
29. Rao C. N. R., Vijayakrishnan V., Aiyer H. N., Kulkarni G. U., Subbanna G. N.: *J. Phys. Chem.* **1993**, *97*, 11157.
30. Kurmaev E. Z., Moewes A., Bureev O. G., Nekrasov I. A., Cherkashenko V. M., Korotin M. A., Ederer D. L.: *J. Alloys Compd.* **2002**, *347*, 213.
31. Yang Z., Wu R.: *Phys. Rev. B* **2003**, *67*, 081403(R).
32. Claus P., Brükner A., Mohr C., Hofmeister H.: *J. Am. Chem. Soc.* **2000**, *122*, 11430.
33. Sanchez A., Abbet S., Heiz U., Schneider W.-D., Häkkinen H., Barnett R. N., Landman U.: *J. Phys. Chem., A* **1999**, *103*, 9573.
34. Kitada M.: *Thin Solid Films* **1994**, *250*, 111.